Atmos. Meas. Tech., 18, 1325–1338, 2025
https://doi.org/10.5194/amt-18-1325-2025

Atmospheric Measurement Techniques
Open Access
EGU

JAXA Level 2 cloud and precipitation microphysics retrievals based on EarthCARE radar, lidar, and imager: the CPR_CLP, AC_CLP, and ACM_CLP products

Kaori Sato[1], Hajime Okamoto[1], Tomoaki Nishizawa[2], Yoshitaka Jin[2], Takashi Y. Nakajima[3], Minrui Wang[3], Masaki Satoh[4], Woosub Roh[4,5], Hiroshi Ishimoto[6], and Rei Kudo[6]

[1]Research Institute for Applied Mechanics, Kyushu University, Fukuoka, 816-8580, Japan
[2]Earth System Division, National Institute for Environmental Studies, Tsukuba, 305-8506, Japan
[3]Research and Information Center, Tokai University, Kanagawa, 2591292, Japan
[4]Atmosphere and Ocean Research Institute, The University of Tokyo, Chiba, 2778564, Japan
[5]Tokyo University of Marine Science and Technology, Tokyo, 1358533, Japan
[6]Department of Observation and Data Assimilation Research, Meteorological Research Institute, Japan Meteorological Agency, Tsukuba, 305-0052, Japan

Correspondence: Kaori Sato (sato@riam.kyushu-u.ac.jp)

Received: 3 June 2024 – Discussion started: 11 June 2024
Revised: 27 October 2024 – Accepted: 17 December 2024 – Published: 14 March 2025

Abstract. This study introduces the primary products and features of active-sensor-based Level 2 cloud microphysics products of the Japanese Aerospace Exploration Agency (JAXA; i.e., the cloud radar standalone cloud product (CPR_CLP), the radar–lidar synergy cloud product (AC_CLP), and the radar–lidar–imager cloud product (ACM_CLP)). Combined with the 94 GHz Doppler cloud profiling radar (CPR), 355 nm high-spectral-resolution lidar (Atmospheric Lidar, ATLID) and Multi-Spectral Imager (MSI), these products provide a detailed view of the transitions of cloud particle categories and their size distributions. Simulated EarthCARE Level 1 data mimicking actual global observations were used to assess the performance of the JAXA Level 2 cloud microphysics product. Evaluation of the product revealed that the retrievals reasonably reproduced the vertical profile of the modeled microphysics. Further validation of the products is planned for post-launch calibration and validation. Velocity-related JAXA Level 2 products (i.e., CPR_VVL, AC_VVL, and ACM_VVL) such as hydrometeor fall speed and vertical air velocity will be described in a future paper.

1 Introduction

With advances in high-resolution global cloud-resolving models for climate simulations, there is increasing interest in the observation of global vertical air velocity and cloud property information. Vertical-air-velocity distributions are important for hydrometeor formation (Sullivan et al., 2016) and cloud dynamics, and EarthCARE will provide the first dense global observations. A method for the simultaneous retrieval of vertical air velocity, particle sedimentation velocity, and microphysics using similar variables obtainable by the EarthCARE Cloud Profiling Radar (CPR) and Atmospheric Lidar (ATLID) has been developed and tested using the Equatorial Atmospheric Radar (Sato et al., 2009). Information derived using this method was used to investigate ice water content in relation to convective activity to evaluate an atmospheric general circulation model (Sato et al., 2010). It is anticipated that analyses of EarthCARE data will be useful for quantifying the role of vertical air velocity in determining cloud properties and lifetime. The lidar depolarization measurement is a strong indicator of particle phase, shape, and orientation (Yoshida et al., 2010). The radar–lidar synergy algorithm with a specular reflection mode investigated the mass mixing ratio of oriented plates (2D types) and randomly oriented crystals (3D ice) within

clouds (Okamoto et al., 2010) and ice precipitation (Sato and Okamoto, 2011) at each vertical grid from CloudSat and Cloud Aerosol Lidar and Infrared Pathfinder Satellite Observations (CALIPSO) data. The recent development of numerical simulations of lidar backscattering for interpreting 355 nm high-spectral-resolution polarization lidar (HSRL) measurements has demonstrated the possibility of deriving more specific ice habit category information from EarthCARE, in addition to the cloud phase and 2D/3D ice category. Measurements from ground-based HSRL support such theoretical studies (Jin et al., 2020, 2022). These unique aspects are incorporated into active-sensor-based Japanese Aerospace Exploration Agency (JAXA) Level 2 (L2) cloud algorithms to create products that are beneficial for investigating cloud formation and cloud precipitation processes. A preliminary study of the JAXA L2 cloud product using available satellite data produced exciting results, displaying a unique geographical preference for the occurrence and height-dependent characteristics of different ice habit categories (Sato and Okamoto, 2023). Each component of the EarthCARE JAXA L2 products should significantly increase our understanding of the coupling of cloud microphysics, radiation, and dynamics.

This paper is organized as follows. Section 2 provides an overview of active-sensor-based JAXA L2 cloud products and simulated EarthCARE Level 1 (L1) data. The JAXA L2 cloud product is demonstrated and assessed in Sect. 3. Section 4 summarizes the results and outlines future expectations for EarthCARE, which was successfully launched into orbit on 28 May 2024 (15:20 LT).

2 Data and description

2.1 Overview of JAXA Level 2 cloud microphysics products

2.1.1 Primary cloud products

Standard cloud property (CLP) products (i.e., the CPR standalone CPR_CLP product, CPR–ATLID synergy AC_CLP product, and CPR–ATLID–MSI synergy ACM_CLP product) include a cloud mask, cloud particle type, cloud particle habit category, cloud microphysics, cloud optical thickness, and cloud water/ice paths (Table 1) (Eisinger et al., 2024). The microphysical properties of all hydrometeor types in the standard products are reported in the cloud microphysics product, and precipitation-sized particles are not separated into precipitation products. JAXA L2 research cloud products include velocity-related products such as sedimentation velocity and vertical air velocity (Sato et al., 2009), which are designated CPR_VVL, AC_VVL, and ACM_VVL, and precipitation-only products (e.g., rain and snow rates; CPR_RAS, AC_RAS, and ACM_RAS) (Table 1). Details of these research products will be reported in a future paper. All products are reported using the Joint Standard Grid (JSG) with 1 km horizontal and 100 m vertical grid spacing. Note that CPR_CLP, AC_CLP, and ACM_CLP are produced with and without the use of L2 CPR Doppler velocity to show the effect of additional information obtained from Doppler velocity. The version without Doppler velocity will eventually be updated based on the version using Doppler velocity. Similarly, research products will be developed through RAS and VVL, and results fulfilling the release criteria may be added to the standard products (i.e., CPR_CLP, AC_CLP, and ACM_CLP) for release.

2.1.2 Rationale for producing three products

The CPR standalone (CPR) algorithm is considered to produce the simplest and most stable products, which are not affected by the observation and retrieval performance of other sensors, though they exhibit relatively higher uncertainty due to the small number of observables. The CPR–ATLID synergy (AC) cloud algorithm and the CPR–ATLID–MSI (ACM) algorithm are generally considered to produce more reliable estimates of cloud microphysics and can handle more complicated scenes in terms of cloud phase with more observables and greater sensitivity. Notably, the degree of improvement in multi-sensor retrievals can be affected by many factors (e.g., day–night differences in ATLID and MSI observations).

The JAXA L2 cloud microphysics algorithms for the CPR standalone, two-sensor, and three-sensor synergy products share the same basic algorithms and assumptions. Less synergetic algorithms are developed and trained with more synergetic algorithms (e.g., the CPR standalone algorithm relative to the two- and three-sensor algorithms and the two-sensor algorithm relative to the three-sensor algorithm). A comparison of the three products and careful investigation of the causes underlying the differences in the retrieval results according to different synergy levels will contribute to the development of better algorithms and more reliable global cloud microphysical products. The release of these three products by JAXA supports the development of retrieval algorithms, allowing for the consistent treatment and integration of comprehensive long-term, spatially dense observations from active sensors on various platforms with differing sensitivity levels to create homogenous microphysics data. Collocated lidar and cloud radar measurements will not always be possible in future missions; therefore, single-sensor algorithms that are consistent with synergetic algorithms are needed (e.g., to process cloud radar data from CloudSat, EarthCARE, and future missions with single CPR measurements).

2.1.3 Summary of available information, challenges, general approaches, and additional information used to constrain retrievals

For cloud microphysics, CPR_CLP and ACM_CLP share the same basic algorithm architecture as AC_CLP, whereas in CPR_CLP, the ATLID observables are simulated based on observations to drive AC_CLP-like retrieval. ACM_CLP has additional steps to handle inputs from the MSI. Further, the framework of ice and water microphysics retrieval algorithms has a similar structure. For these algorithms, a maximum of two size modes in each JSG are used to treat the coexistence of cloud ice and snow in the ice phase, cloud liquid and ice (or snow) in the mixed phase, and cloud liquid and liquid precipitation in the liquid phase. Cloud ice microphysics are generally retrieved by CPR–ATLID synergy, whereas ice and liquid precipitation are often retrieved by CPR alone due to the attenuation of ATLID signals, and cloud liquid is retrieved through either ATLID-only or CPR-only retrieval schemes, as lidar and cloud radar are considered to be sensitive to different portions of the particle size distribution, particularly for water clouds.

Cloud microphysics retrieval in CPR-only regions involves challenges in producing effective radius (r_{eff}) and ice water content (IWC) or liquid water content (LWC) solely from radar reflectivity (Z_{e}) constrained by pulse-integrated attenuation (PIA) when Doppler velocity is not used. The dependence of Z_{e} on cloud microphysical properties reflects cloud physical processes (e.g., Khain et al., 2008). A single size mode cannot explain the transition stage between clouds and precipitation (Krasnov and Russchenberg, 2002). Therefore, a methodology to consider two size modes in each JSG is developed for a better interpretation of Z_{e} profiles in both ice and liquid clouds. Z_{e} is less sensitive to cloud particles in the presence of precipitation particles in ice or liquid clouds, and Z_{e} is less sensitive to liquid cloud particles in the presence of ice particles in mixed-phase clouds. In such cases, the additional information of MSI optical thickness is effective for constraining cloud r_{eff} and LWC (or IWC) derived from AC_CLP in the ACM_CLP scheme. For CPR_CLP, the same microphysics retrieval scheme employed by AC_CLP for the cloud region detected by CPR only is used. To run the AC_CLP scheme, the statistical relationships between lidar observables and Z_{e} for the water and ice phases are derived from long-term CALIPSO and CloudSat observations and applied to create ATLID-like observations (Okamoto et al., 2020) as a function of Z_{e}, which is fully attenuated in optically thick regions, realistically recreating observations. The current version of ATLID-like inputs will be replaced by inputs directly derived from ATLID and CPR observations. Currently, the ATLID-like input is used for only for the ice phase. For liquid cloud microphysics, ATLID-only and CPR-only retrievals are obtained and combined in the AC_CLP algorithm due to the differing sensitivity of the sensors to cloud particle size. For CPR_CLP, the CPR-only retrieval without the ATLID-like input is conducted for liquid cloud microphysics.

2.2 Processing flow of the JAXA Level 2 cloud microphysics product

Figure 1 shows the flow of the L2 cloud products. The JAXA L2 Echo algorithm processes CPR L1 data and was developed by the National Institute of Information and Communications Technology (NICT). The major outputs from the JAXA L2 Echo product to CPR_CLP, AC_CLP, and ACM_CLP are radar reflectivity factor (Z_{e}), Doppler velocity (V_{D}), normalized radar cross-section (σ_0), pulse-integrated attenuation (PIA), gaseous attenuation, clutter mask, and quality flags. The inputs from the JAXA L2 ATLID product (Nishizawa et al., 2024) to the AC_CLP and ACM_CLP algorithms are the L2 ATLID observables (i.e., extinction coefficient, α_{ext}; attenuated backscattering coefficient, β_{att}; true backscattering coefficient, β; and depolarization ratio, δ) and their aerosol and cloud components (Kudo et al., 2016, 2023), ATLID-only cloud mask and cloud type (Okamoto et al., 2024a). Aerosol extinction is used to handle attenuation due to aerosols above the cloud layers.

The L2 cloud algorithms are processed in the following order: CPR_CLP, AC_CLP, and ACM_CLP. The cloud mask, cloud type, and cloud particle category products from each algorithm are passed to the high-order synergy algorithms. The CPR-only cloud mask, cloud type, and cloud particle category products from L2a CPR_CLP are used as input for the L2b AC_CLP algorithm, and these products derived by CPR only are combined with the ATLID-only cloud mask, cloud type, and cloud particle category to produce CPR–ATLID synergy products. These products are then applied to the AC_CLP algorithm to derive cloud microphysics products. The AC_CLP cloud mask, cloud type, and cloud particle category products are further passed to the ACM_CLP algorithm and used for three-sensor microphysics retrieval. The MSI is not currently used to improve the cloud mask, type, and category products; therefore, these products from ACM_CLP are the same as those from AC_CLP. The inputs from JAXA L2 MSI products to ACM_CLP are the optical thicknesses of the ice and liquid phases (Nakajima et al., 2019; Wang et al., 2023), which are used to constrain CPR_CLP and AC_CLP microphysics estimates. The JAXA Level 2 cloud product is further handled by the JAXA L2 four-sensor radiation products (Yamauchi et al., 2024). Details of the relationships among JAXA Level 2 algorithms and products have been provided by Okamoto et al. (2024b).

2.3 Description of the JAXA Level 2 cloud microphysics product

The following section provides a brief overview and highlights of the standard JAXA L2 cloud microphysics products.

Table 1. Primary parameters of the Japanese Aerospace Exploration Agency (JAXA) Level 2 (L2) standard (ST) and research (ER, LR) active-sensor-based cloud products, including the standalone products (CPR_CLP, CPR_RAS, and CPR_VVL), CPR–ATLID synergy cloud products (AC_CLP, AC_RAS, and AC_VVL), and CPR–ATLID–MSI products (ACM_CLP, ACM_RAS, and ACM_VVL). The ER and LR products are processed by the JAXA Earth Observation Research Center Research and Application System and JAXA laboratories, respectively. The standard CPR_CLP and AC_CLP products will be updated with the use of Doppler velocity, and the ACM_CLP cloud property products updated with the use of Doppler velocity will be provided by ACM_CDP as research (LR) products. ATLID: Atmospheric Lidar; CPR: Cloud Profiling Radar; MSI: Multi-Spectral Imager.

Standard product	Description	L2a CPR	L2b CPR–ATLID	L2b CPR–ATLID–MSI
		CPR_CLP*	AC_CLP*	ACM_CLP**
Cloud mask	Cloud and precipitation (described in Okamoto et al.,	√ST	√ST	√ST
Cloud particle type	2024a) clear, warm water, supercooled water, 3D ice, 2D plate,mixture of 3D ice and 2D plate, liquid drizzle, mixed-phase drizzle, rain, snow, water + liquid drizzle, water + rain, mixed phase, melting layer	√ST	√ST	√ST
Cloud particle category	Cloud particle habit categories (2D plate, 2D column, bullet rosette/3D aggregates, droxtal/compact, Voronoi/irregular, fractal, liquid-phase types from cloud particle type product)	√ST	√ST	√ST
Cloud water effective radius	Cloud and precipitation; both liquid-phase and	√ST	√ST	√ST
Cloud ice effective radius	ice-phase microphysics are reported at each vertical	√ST	√ST	√ST
Cloud water content	grid (precipitation-only products are provided by	√ST	√ST	√ST
Cloud ice content	CPR_RAS, AC_RAS, and ACM_RAS)	√ST	√ST	√ST
Total cloud water number concentration		√ST	√ST	√ST
Total cloud ice number concentration		√ST	√ST	√ST
Cloud effective radius 1 Cloud effective radius 2	Subcategory products to infer particle size distribution of cloud and precipitation cloud phase 1 and 2:	√ST	√ST	√ST
Cloud water content 1 Cloud water content 2	(0) not retrieved, (1) water, (2) ice, (−9) clear. Combinations of ice + ice, water + water, and	√ST	√ST	√ST
Cloud number concentration 1 Cloud number concentration 2	ice + water are possible. Cloud effective radius, water content, and number concentration corresponding to	√ST	√ST	√ST
Cloud phase 1 Cloud phase 2	cloud phase 1 and 2 are reported at each vertical grid.	√ST	√ST	√ST
Optical thickness	Liquid + ice phase	√ST	√ST	√ST
Cloud water path		√ST	√ST	√ST
Cloud ice water path		√ST	√ST	√ST
Rain and snow properties (rain/snow rate, rain/snow water content)	Vertical profile	√ER	√ER	√LR
			AC_MRA	
Mass ratios of 2D plates	Okamoto et al. (2010)		√ER	
		CPR_VVL	AC_VVL	ACM_VVL
Cloud Doppler velocity	In-cloud Doppler velocity with folding correction after applying cloud mask	√ER	√ER	√LR
Total terminal velocity of cloud	Mean terminal velocity of cloud and precipitation particles	√ER	√ER	√LR
Cloud terminal velocity 1 Cloud terminal velocity 2	Terminal velocity corresponding to cloud effective radius 1 and cloud effective radius 2	√ER	√ER	√LR
Vertical air velocity	In-cloud vertical air velocity	√ER	√ER	√LR

* Standard CPR_CLP and AC_CLP products will be updated with the use of Doppler velocity.
** Standard CPR–ATLID–MSI cloud property products with the use of Doppler velocity are provided by ACM_CDP as research (LR) products.

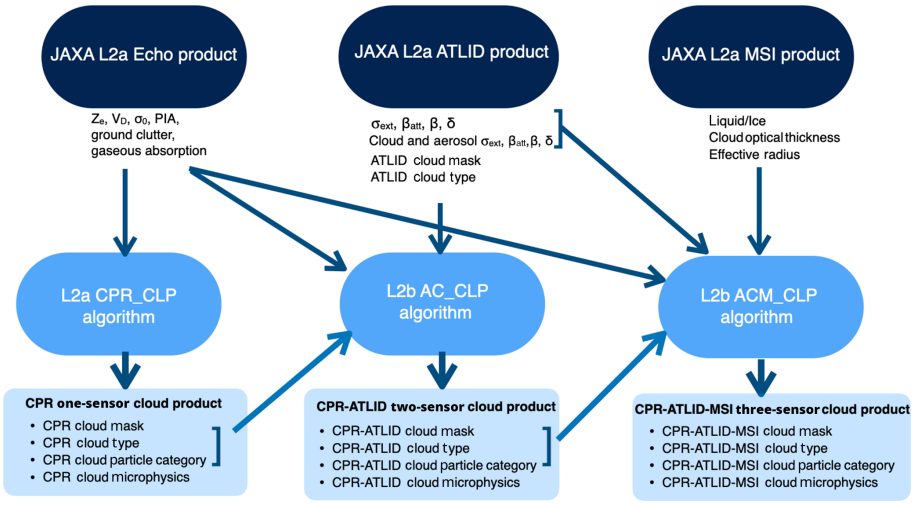

Figure 1. Flow of the Japanese Aerospace Exploration Agency (JAXA) Level 2 (L2) cloud products, including the standalone product (CPR_CLP), the CPR–ATLID synergy cloud product (AC_CLP), and the CPR–ATLID–MSI product (ACM_CLP). The JAXA L2 Echo product contains the radar reflectivity factor (Z_e), Doppler velocity (V_D), normalized radar cross-section (σ_0), and pulse-integrated attenuation (PIA). The JAXA L2 ATLID product contains the extinction coefficient (α_{ext}), attenuated (β_{att}) and true backscattering coefficient (β), and depolarization ratio (δ). ATLID: Atmospheric Lidar; CPR: Cloud Profiling Radar; MSI: Multi-Spectral Imager.

2.3.1 Preprocessing for cloud microphysics retrieval

Cloud mask

The ATLID-only cloud mask is processed by the ATLID_CLA algorithm (Nishizawa et al., 2024), the CPR-only cloud mask is processed by the CPR_CLP algorithm (Okamoto et al., 2024a), and the MSI-only cloud mask is processed by the MSI_CLP algorithm (Nakajima et al., 2019). For ATLID, the aerosol, cloud, and surface components are discriminated from clear pixels when the Mie backscattering coefficient is significant compared to the noise level (Nishizawa et al., 2024). A cloud mask scheme is then applied; this scheme includes a vertically variable threshold value for the Mie backscattering coefficient (or particle backscattering coefficient when the Rayleigh backscattering coefficient is significant), as well as a spatial continuity test to exclude noisy pixels. The lack of a sufficient surface signal is used to identify fully attenuated ATLID pixels below aerosol or cloud layers. Similarly, the CPR cloud mask scheme considers noise level, continuity testing, and surface echo information to determine sufficient radar echo power for cloud and precipitation analysis, as well as full attenuation of the radar signal. The AC_CLP synergy cloud mask scheme merges the single active-sensor cloud mask results from ATLID_CLA and CPR_CLP and then flags cloudy pixels in ATLID, CPR, or both. MSI cloud mask information is not used for the ACM_CLP cloud mask. The AC_CLP and ACM_CLP cloud mask products are currently identical.

Cloud type

The ATLID cloud type scheme (ATLID_CLA) uses δ, β_{att}, and temperature to identify the cloud phase and ice particle orientation, which is designated as two-dimensional (2D) ice, three-dimensional (3D) ice, or mixed 2D and 3D ice (Okamoto et al., 2024a). The CPR cloud type scheme (CPR_CLP) mainly uses Z_e (along with its vertical profile) and temperature to discriminate the hydrometeor phase, ice particle orientation, precipitation type (snow, drizzle, or rain), and melting layer (Okamoto et al., 2024a). The AC_CLP synergy cloud type scheme combines ATLID_CLA with CPR_CLP and reclassifies the cloud type when estimates from the two sensors differ according to the classification rule specified by Kikuchi et al. (2017). The differing particle size sensitivity of CPR and ATLID aids in the identification of mixed-phase clouds and mixed cloud precipitation types (i.e., cloud water + drizzle or cloud water + rain). The ACM_CLP and AC_CLP cloud types are identical. In addition, Doppler velocity will be used to improve differentiation between snow and rain and between cloud and drizzle. Further details of the cloud mask and cloud particle type products have been reviewed by Nishizawa et al. (2024) and Okamoto et al. (2024a).

Cloud particle category (CPC)

After applying the cloud mask and cloud phase discrimination schemes (Okamoto et al., 2024a), one of the main products of the EarthCARE JAXA L2 cloud product is the cloud particle category product, which enables more detailed comprehensive exploration of the ice particle habit category

contained within each JSG grid. Among cloud particle categories, the liquid-phase types are the same as those in the cloud type product (see "Cloud type" in Sect. 2.3.1). Ice particles are further categorized based on ATLID lidar ratio and depolarization ratio diagrams (Okamoto et al., 2019, 2020; Sato and Okamoto, 2023). This information is anticipated to be instrumental for general remote sensing applications (Van Diedenhoven, 2018; Letu et al., 2016) and the development of ice optical parameterization (Li et al., 2022) and hydrometeor sedimentation velocity parameterization for use in numerical models. The retrieved ice particle habit categories include horizontally oriented 2D plates and their assemblages, 2D columns and their assemblages, bullet rosettes and 3D-oriented aggregate types, droxtal/compact types, Voronoi/irregular/roughened types, and fractal-type snow aggregates (Ishimoto, 2008; Ishimoto et al., 2012). The ATLID-only CPC is used to train the CPR-based algorithm for ice particle category retrieval from Z_e and temperature information in regions with CPR-only measurements. The CPR-only CPC product is obtained from CPR_CLP. CPR_CLP and ATLID-only CPC are combined to produce the synergy AC_CLP CPC product. For ice categories, ATLID-only CPC estimates are used when both CPR_CLP CPC and ATLID-only CPC estimates are available for the same JSG grid. The Doppler velocity will be further used to improve category identification, particularly for snow types (e.g., graupel or hail).

2.3.2 Cloud microphysics

In CPR_CLP, ACP_CLP, and ACM_CLP, forward models corresponding to the derived cloud particle categories are used to analyze the observations from each sensor, and microphysics corresponding to each category are thus obtained. The single-scattering properties of ice particles with various shapes and orientations are calculated using integral equation methods with physical optics (Borovoi et al., 2012) and modified geometrical optics integral optics methods (Masuda et al., 2012) for ATLID specification (Okamoto et al., 2019), as well as discrete dipole approximation and finite-difference time domain (FDTD) methods for CPR wavelength (Sato and Okamoto, 2011; Ishimoto, 2008; Ishimoto et al., 2012). Mie theory is used for the liquid phase, and multiple-scattering effects are estimated based on Sato et al. (2018, 2019).

The total effective radius for cloud and precipitation information is given as

$$r_{\mathrm{eff}} = \int r_{\mathrm{eq}}^3 \frac{\mathrm{d}n(r_{\mathrm{eq}})}{\mathrm{d}r_{\mathrm{eq}}} \mathrm{d}r_{\mathrm{eq}} \Big/ \int r_{\mathrm{eq}}^2 \frac{\mathrm{d}n(r_{\mathrm{eq}})}{\mathrm{d}r_{\mathrm{eq}}} \mathrm{d}r_{\mathrm{eq}}, \quad (1)$$

where r_{eq} is the melted mass equivalent radius to a sphere, and $\mathrm{d}n/\mathrm{d}r_{\mathrm{eq}}$is the size distribution function. For both ice- and liquid-phase clouds, a maximum of two different particle size distributions ($i = 1, 2$) can be considered within one JSG grid to handle the presence of cloud and precipitation modes, i.e., $\frac{\mathrm{d}n(r_{\mathrm{eq}})}{\mathrm{d}r_{\mathrm{eq}}} = \sum_{i=1}^{2} \frac{\mathrm{d}n_i(r_{\mathrm{eq}})}{\mathrm{d}r_{\mathrm{eq}}}$. The corresponding effective radius is given as

$$r_{\mathrm{eff},i} = \int r_{\mathrm{eq}}^3 \frac{\mathrm{d}n_i(r_{\mathrm{eq}})}{\mathrm{d}r_{\mathrm{eq}}} \mathrm{d}r_{\mathrm{eq}} \Big/ \int r_{\mathrm{eq}}^2 \frac{\mathrm{d}n_i(r_{\mathrm{eq}})}{\mathrm{d}r_{\mathrm{eq}}} \mathrm{d}r_{\mathrm{eq}} \quad (i = 1, 2). \quad (2)$$

For $\mathrm{d}n_i/\mathrm{d}r_{\mathrm{eq}}$, a modified gamma size distribution,

$$\frac{\mathrm{d}n_i(r_{\mathrm{eq}})}{\mathrm{d}r_{\mathrm{eq}}} = \frac{N_{\mathrm{o},i}}{\Gamma(p) r_{\mathrm{m},i}} \left(\frac{r_{\mathrm{eq}}}{r_{\mathrm{m},i}}\right)^{p-1} \exp\left(-\frac{r_{\mathrm{eq}}}{r_{\mathrm{m},i}}\right) \quad (i = 1, 2), \quad (3)$$

in which r_{m} is the characteristic radius, and the dispersion value is $p = 2$ (Okamoto, 2002; Sato and Okamoto, 2011), is employed for cloud ice, snow, and rain in cold precipitation. A log-normal size distribution,

$$\frac{\mathrm{d}n_i(r_{\mathrm{eq}})}{\mathrm{d}r_{\mathrm{eq}}} = \frac{N_{\mathrm{o},i}}{\sqrt{2\pi} r_{\mathrm{eq}} \ln\sigma} \exp\left\{-\frac{\left[\ln\left(r_{\mathrm{eq}}/r_{\mathrm{o},i}\right)\right]^2}{2(\ln\sigma)^2}\right\} \quad (i = 1, 2), \quad (4)$$

in which r_{o} is the mode radius, and the standard deviation of the distribution is $\sigma = 1.5$ (Okamoto, 2002), is assumed for warm water, supercooled liquid, and warm precipitation.

In the following, general approaches for cloud microphysics retrievals are explained based on the AC_CLP cloud microphysics algorithm. These approaches are common to CPR_CLP and ACM_CLP cloud microphysics algorithms.

Ice cloud microphysics

For ice clouds, a lidar-only cloud region, lidar–radar overlap cloud region, and radar-only region generally exist for ice and liquid precipitation. An algorithm to retrieve microphysical properties that considers a mixture of two particle types at maximum (i.e., 2D and 3D ice) has been developed for ice cloud regions observed with CloudSat and CALIPSO synergy (Okamoto et al., 2010) using Z_e, the attenuated backscattering coefficient β, and the depolarization ratio. A framework to extend the applicability of the microphysics retrieval algorithm from the cloud region to the entire precipitation region in the vertical column was developed to efficiently reflect information from the lidar–radar overlap region in the microphysics retrieved in the CloudSat- or CALIPSO-only region (Sato and Okamoto, 2011, 2020). The relationships between microphysical properties (r_{eff} and IWC) and β or Z_e in the vertical cloud grids of the lidar–radar overlap region were derived for each profile and used to estimate the microphysical properties in the radar- or lidar-only cloud region (Sato and Okamoto, 2011). The EarthCARE JAXA L2 cloud microphysics retrieval algorithms extend these algorithms in the following three aspects: (1) the spatial variability in the microphysics and observables are considered to derive more reliable relationships among cloud microphysics and observables; (2) the microphysics estimates in the ice precipitation region far from the lidar–radar overlap region of a precipitation system are further improved by extending the microphysics estimates from the precipitation region upward rather than downward from the lidar–radar region (Heymsfield et al., 2018); and (3) the single-size mode

for cloud ice is considered for the lidar-only cloud region and the lidar–radar overlap cloud region, while two different size modes for cloud ice and ice precipitation (snow) are considered for the CPR-only region existing from the bottom altitude of the lidar–radar overlap region to the top altitude of the melting level. The PIA is used to correct the attenuation of Z_e (Iguchi et al., 2000).

Specifically, for (1), the L2 cloud microphysics algorithm uses r_{eff} and IWC for all horizontal and vertical grids within the radar–lidar overlap region embedded in each cloud system to obtain robust relationships of cloud microphysics with Z_e and β (e.g., Z_e–IWC relationships, $Z_{e,1} = a_1\ \mathrm{IWC}_1^{b1}$, are determined for each record, where Z_e is in $\mathrm{mm^6\,m^{-3}}$, and IWC is in $\mathrm{g\,m^{-3}}$). These relationships are derived for each record using all data within each cloud system (or within a single EarthCARE orbit frame when a sufficient number of points cannot be obtained to derive the statistics) weighted by distance from the target profile record and are used to provide initial estimates of cloud ice microphysics based on Z_e or β in the CPR-only (ice cloud and ice precipitation) or ATLID-only (ice cloud) regions, respectively.

For (2), the relationship between the microphysics and observables is expected to change from the cloud region to the precipitation region. Because lidar signals are fully attenuated in the optically thick precipitation region, new relationships for ice precipitation are derived using CPR data. In this process, CPR data at melting levels or layers around the ice–liquid interfaces of a precipitation system are used. At the top of the melting level, it is assumed that only the precipitation mode exists ($Z_e = Z_{e,2}$), and during melting, the mass in each size bin (i.e., r_{eff}) remains constant across several successive layers (Heymsfield et al., 2018). For a given r_{eff}, $\mathrm{dB}Z_e$ changes due to the different scattering properties for ice and liquid. Therefore, r_{eff} and IWC (or LWC) are derived, and the relationships ($Z_{e,2} = a_2\ \mathrm{IWC}_2^{b2}$) can be established for ice precipitation (snow), holding the coefficient b_2 at the value derived in (1) ($b_2 = b_1$) for each record.

For (3), $Z_{e,1}$ and $Z_{e,2}$ for the two size modes (cloud ice and snow) in the CPR-only ice precipitation region at each vertical grid ($Z_{e,1} + Z_{e,2} = Z_e$) are determined as follows. The ratio $\mathrm{IWC}_2 / (\mathrm{IWC}_1 + \mathrm{IWC}_2) = \mathrm{IWC}_2 / \mathrm{IWC} = A$ increases linearly from 0 at the bottom of the lidar–radar overlap region to 1 at the top of the melting level. A is given as $A = \int_h^{h_t} Z_e\,\mathrm{d}h \,/\, \int_{h_m}^{h_t} Z_e \mathrm{d}h$, with a range of 0 to 1, where the integrated Z_e from the bottom altitude of the lidar–radar overlap region (h_t) to a certain altitude h below h_t within the CPR-only ice precipitation region ($\int_h^{h_t} Z_e \mathrm{d}h$) is normalized using the value integrated to the melting level altitude h_m ($\int_{h_m}^{h_t} Z_e \mathrm{d}h$). As the Z_e–IWC relationships for both cloud ice and snow are derived, determining the vertical profile of $\mathrm{IWC}_2 / \mathrm{IWC}$ is equivalent to providing the relationship between $Z_{e,1}$ and $Z_{e,2}$ for each vertical grid. Therefore IWC_i, $r_{eff,i}$ ($i = 1, 2$), and other microphysical properties are derived for each JSG grid (Table 1).

In microphysics retrieval for convective/stratiform rain below the melting level, only the precipitation size mode is assumed to exist. The r_{eff} and LWC obtained at the rain's top altitude of each observation record described in (2) are used to derive the N_o and x values of the Marshall–Palmer size distribution ($\mathrm{d}n/\mathrm{d}D = N_o\, e^{-\Lambda D}$ ($\mathrm{m^{-4}}$), where D is the particle diameter; $\Lambda = x R^{0.21}$ ($\mathrm{cm^{-1}}$); and R is the rain rate in $\mathrm{mm\,h^{-1}}$, which is a function of LWC and r_{eff}) (Marshall and Palmer, 1948). N_o and x are assumed to be constant within the vertical profile for rain in a given record and are used to determine the vertical profiles of LWC and r_{eff} for the modified gamma size distribution associated with each Z_e value in the rain region.

Generally, for the same Z_e, when the mass mixing ratio of the small mode to total IWC is overestimated (underestimated), optical thickness will be overestimated (underestimated); in the three-sensor ACM_CLP algorithm, the mass mixing ratio of the two size modes is further constrained by the optical thickness obtained from the MSI. When only a single size mode is present, the r_{eff} and IWC of the single mode are adjusted to be consistent with MSI optical thickness retrievals. Doppler velocity is expected to effectively improve particle sizing in regions of ice and liquid precipitation, as well as in the breakup of large snow particles during melting (e.g., Fujiyoshi et al., 2023).

Liquid cloud microphysics

A two-size-mode approach similar to the ice cloud microphysics retrieval process is used for water clouds, which considers the coexistence of cloud particles and drizzle. CPR_CLP derives the liquid microphysics corresponding to each size mode from the CPR-only scheme. In AC_CLP and ACM_CLP, for JSG grids with ATLID observables, ATLID δ and β_{att} (or σ_{ext}) are used to derive $r_{eff,1}$ and LWC_1 for cloud water or supercooled water (Sato et al., 2018, 2019; Sato and Okamoto, 2020). As ATLID is expected to provide a better estimate of the cloud mode than CPR, for the CPR and ATLID overlap region, the ATLID cloud microphysics and $Z_{e,1}$ estimate are used for microphysics estimation of the drizzle mode.

In water clouds, in situ and ground-based radar measurements have shown that cloud particles and drizzle-sized particles can coexist above $-35\,\mathrm{dB}Z_e$ (Baedi et al., 2000). Except at very small ($< -35\,\mathrm{dB}Z_e$) and large values of Z_e, where only a single mode is likely to occur, the cloud mode can dominate LWC and r_{eff}, whereas the precipitation mode can dominate Z_e (Baedi et al., 2000; Krasnov and Russchenberg, 2005). For this reason, in general, the dependence of total LWC on Z_e differs significantly from results derived for only cloud particles (LWC_1 and $Z_{e,1}$) or only drizzle-sized particles (LWC_2 and $Z_{e,2}$) (Baedi et al., 2000). PIA is sensitive to total LWC, and in the CPR-only microphysics retrieval scheme, the Z_e–LWC relationship ($Z_e = a\,\mathrm{LWC}^b$, where Z_e is in $\mathrm{mm^6\,m^{-3}}$, and LWC is in $\mathrm{g\,m^{-3}}$) and LWC for the

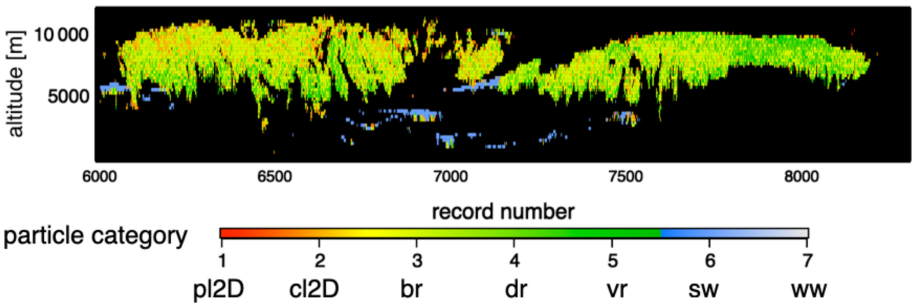

Figure 2. Demonstration of the JAXA L2 ice particle category product reported from the JAXA L2 ATLID product (ATL–CLA). The dominant ice category type is classified into (1) 2D plate (pl2D), (2) 2D column (cl2D), (3) 3D bullet (bullet rosettes, 3D aggregate category) (br), (4) droxtal (dr), and (5) Voronoi (vr) types as well as (6) supercooled water (sw) and (7) warm water (ww). The JAXA EarthCARE L2 cloud algorithms were modified to be applied to A-Train data, and the ice category classification was derived using Cloud-Aerosol Lidar with Orthogonal Polarization (CALIOP).

cloud + drizzle mode for the JSG grids within each record are determined from PIA and Z_e, assuming that $b = 5.17$ (Baedi et al., 2000). The power b_i of the Z_e–LWC relationship for clouds and drizzle is reported to have similar values and assumed to be fixed (i.e., $b_1 \sim 1.17$, Baedi et al., 2000, and Fox and Illingworth, 1997; $b_2 \sim 1.58$, Krasnov and Russchenberg, 2002), while the coefficient a_i in the Z_e–LWC relationship could differ between clouds and drizzle by several orders of magnitude, reflecting the size distribution difference (Khain et al., 2008). As CPR Z_e is more sensitive to the drizzle mode (i.e., $Z_{e,2}$), the a_1 coefficient for the cloud mode is assumed to be initially fixed at a reported value ($a_1 = 0.015$; Baedi et al., 2000), and a_2 is derived for each Z_e and LWC profile, given that $\mathrm{LWC}_1 + \mathrm{LWC}_2 = \mathrm{LWC}$, and $Z_{e,1} + Z_{e,2} = Z_e$. Finally, $Z_{e,i}$, $r_{\mathrm{eff},i}$, LWC_i ($i = 1, 2$), and other microphysical properties such as the number concentration and particle fall speed are derived for the two size modes.

The liquid cloud microphysics are further constrained by the ATLID observables for the AC_CLP and ACM_CLP algorithms and the MSI for the ACM_CLP algorithm. Doppler information will be used to improve the microphysics estimates of the precipitation (drizzle) mode.

2.3.3 Intended use of Doppler measurements for vertical-air-velocity and terminal velocity products

The Doppler velocity is intended to be used in at least two approaches; vertical air velocity is determined by subtracting the Z_e-weighted particle fall speed corresponding to each cloud particle category obtained without the use of Doppler velocity and simultaneous retrieval of vertical air velocity and microphysics through an approach similar to that described by Sato et al. (2009), which considers the difference between the vertical structures of Z_e (reflecting cloud microphysics) and V_D (which is affected by vertical air velocity and cloud microphysics) to extract the vertical-air-velocity component.

2.4 JAXA Joint Simulator-derived EarthCARE L1 data

The performance of the JAXA L2 cloud algorithms was tested using simulated EarthCARE L1 orbit data created by the JAXA Joint Simulator (Roh et al., 2023a, and references therein). These L1 data are created using cloud and precipitation scenes generated by the Nonhydrostatic Icosahedral Atmospheric Model (NICAM) (Satoh et al., 2014) at 3.5 km horizontal resolution and profiles of aerosol species simulated by the NICAM Spectral Radiation–Transport Model. Random errors and noise are added to create CPR and ATLID signals, and the spectral misalignment effect of the visible and near-infrared channels is introduced for the MSI (Roh et al., 2023a) to mimic actual observations. The simulated L1 data for an EarthCARE orbit are divided into 8 frames, and 15 frames, corresponding to nearly 2 orbits, are simulated to include representative cloud and aerosol scenes around the world. All 15 frames are used to evaluate the JAXA L2 cloud product.

3 Demonstration and assessment of JAXA Level 2 cloud product

Figure 2 shows the ice particle category product, which was derived using complementary observations from Cloud-Aerosol Lidar and Infrared Pathfinder Satellite Observations (CALIPSO) and Cloud-Aerosol Lidar with Orthogonal Polarization (CALIOP) (Sato and Okamoto, 2023). The CALIPSO data were combined onto the CloudSat grid with a resolution of 240 m vertically and 1 km horizontally (Kyushu University, KU, CloudSat–CALIPSO merged dataset data; Hagihara et al., 2010). Lidar ratio and depolarization ratio information from ATLID may offer a more robust classification of ice particle categories and orientations, and long-term

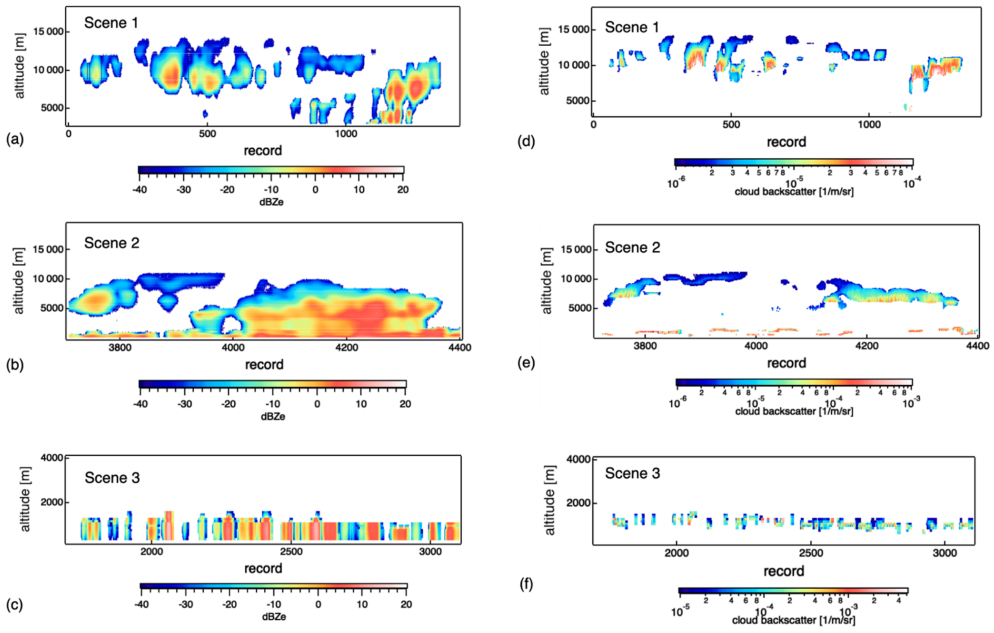

Figure 3. Inputs of CPR Z_e measurements **(a, b, c)** simulated using the JAXA Joint Simulator and ATLID L2a cloud backscatter product **(d, e, f)** for different cloud scenes. **(a, d)** Scene 1 is a cirrus case, **(b, e)** scene 2 is a case with more ice precipitation, and **(c, f)** scene 3 is dominated by the liquid phase.

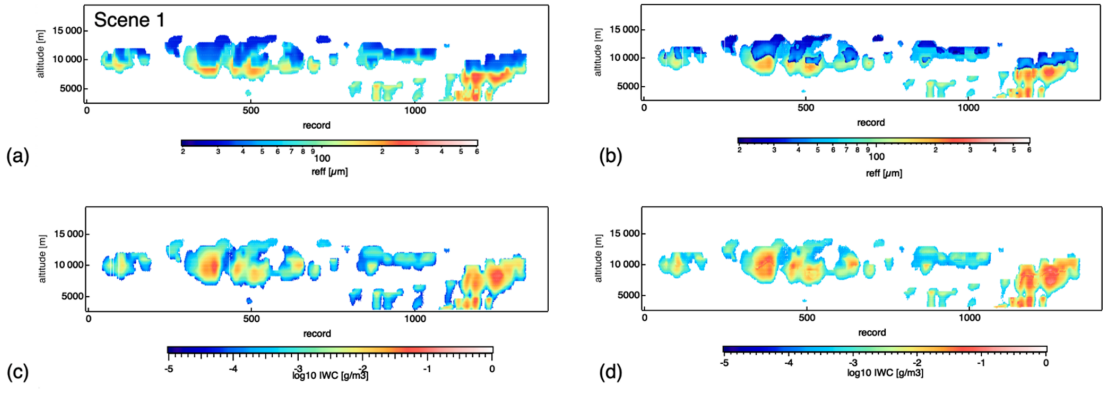

Figure 4. Time–height cross-section of **(a, c)** simulated and **(b, d)** retrieved effective radius and total water content for an ice-phase case corresponding to scene 1 in Fig. 4a.

analysis of these products using CALIOP and ATLID observations will increase the reliability of the product (Okamoto et al., 2020). The EarthCARE L2 data will be provided at 100 m vertical resolution.

Cloud microphysics retrieved from the simulated EarthCARE L1 data are compared with the truth. For comparison, we used the standard AC_CLP products. Figure 3 shows an example of the time–height cross-section of the simulated CPR measurements and the ATLID L2a cloud backscatter for a cirrus case (scene 1), snow precipitation (scene 2), and a liquid-phase cloud scene (scene 3). Overall, there was good consistency between the simulated and retrieved cloud water contents and effective radius, where the standard AC_CLP retrievals reproduced vertical variation in the microphysical properties seen in the model reasonably well (Figs. 4–6).

We also performed a one-to-one comparison of retrieved (ret) and modeled (JS) effective radius ($r_{\mathrm{eff,ret}}$ and $r_{\mathrm{eff,JS}}$), ice water content ($\mathrm{IWC_{ret}}$ and $\mathrm{IWC_{JS}}$), and liquid water content ($\mathrm{WC_{ret}}$ and $\mathrm{WC_{JS}}$) at each JSG grid for AC_CLP using all 15 EarthCARE frames of the simulated observation data (Figs. 7 and 8). The results showed that for both the ice and liquid phases, the majority of the retrieved population of r_{eff} and water content lay close to the 1 : 1 line. For the ice phase, the slopes of the regression lines were generally around 0.8, and ice water content had a mean relative error of about 14.5 % and tended to be slightly overestimated when the ice water

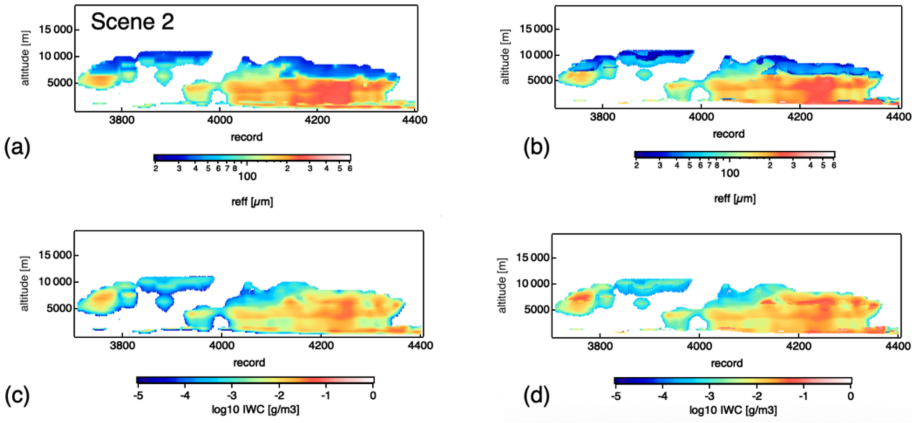

Figure 5. Same as Fig. 5 but for the ice microphysics corresponding to scene 2 in Fig. 4b.

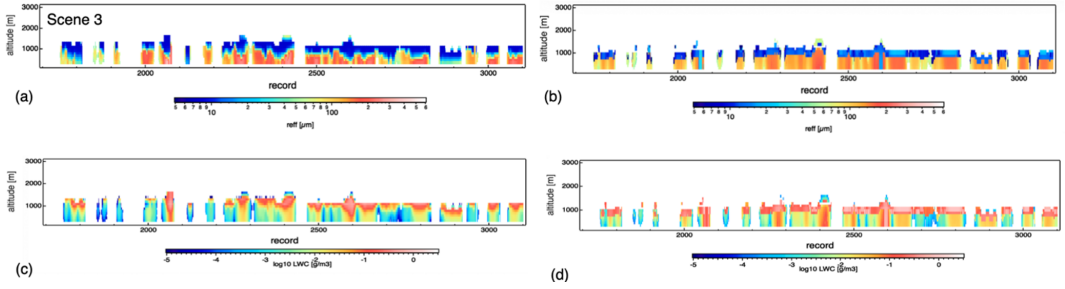

Figure 6. Time–height cross-section of **(a, c)** simulated and **(b, d)** retrieved effective radius and total water content for a liquid-phase case corresponding to scene 3 in Fig. 4c.

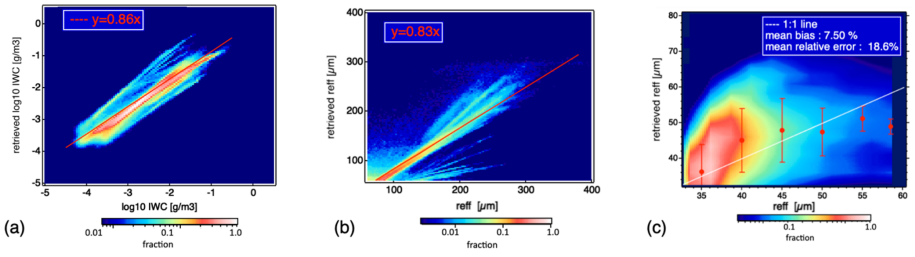

Figure 7. Scatterplot of retrieved and modeled **(a)** ice water content and **(b, c)** ice-phase effective radius. Solid red and white lines correspond to a linear regression line forced through the origin and a 1:1 ratio, respectively. Symbols in **(c)** indicate the mean and standard deviation of retrieved r_{eff}.

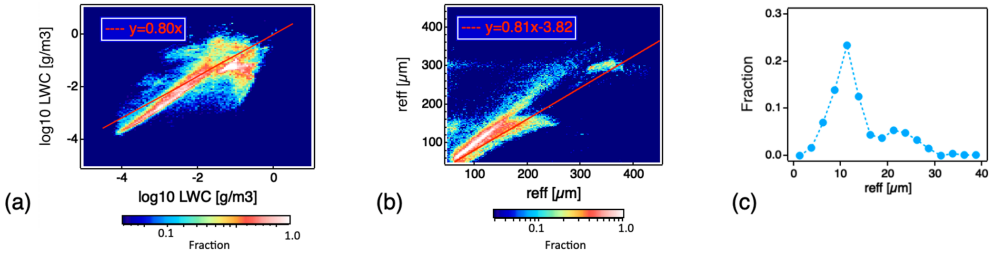

Figure 8. Scatterplot of retrieved and modeled **(a)** liquid water content and **(b)** effective radius of liquid precipitation. The frequency distribution of the retrieved effective radius of cloud particles is shown in **(c)**. Solid lines correspond to a linear regression line.

content was small (Fig. 7a). The effective radius of the ice phase was evaluated at small (Fig. 7c) and large size ranges (Fig. 7b) bounded at 60 µm. In the model, three modes (i.e., ice cloud particles, snow, and graupel) contributed to the effective radius for the ice phase. Despite such complexity, the mean relative error in the effective radius retrievals for the larger size range was about 28.9 %, and the mean relative errors and the mean bias of the effective radius retrievals for the smaller size range were about 18.6 % and 7.5 %, respectively.

The liquid water content retrievals for the water clouds were able to track the change in the liquid water content and corresponded relatively well with the model truth. A larger scatter around the truth was observed at a larger liquid water content range, which was biased low. Further analysis of the model suggested that this could have in part occurred when liquid cloud particles made a major contribution to the water content but a negligible contribution to Z_e and its vertical structure, which in some cases the algorithm slightly misinterpreted when determining their contributions in the CPR-only regions. The slopes of the regression lines were also around 0.8 for both liquid water content and effective radius of liquid precipitation (Fig. 8a, b). For the smaller size range, the frequency distribution of the retrieved effective radius was examined since the liquid cloud particles in the model has a constant effective radius of 8 µm (Fig. 8c). It was observed that the retrieved peak size was close to the model truth and was around 10 µm, which was an overestimation of about 2 µm, and a smaller fraction of drizzle-sized particles was also retrieved. In the future, we will further investigate the improvement in the microphysics retrieval when the ACM_CLP algorithm with CPR–ATLID–MSI synergy is applied to the simulated EarthCARE L1 data.

4 Summary and expectations

This study introduces the active-sensor-based JAXA L2 cloud product, which is produced using three different algorithm-processing chains. The L2a CPR_CLP chain produces the standalone CPR cloud product; L2b AC_CLP produces the CPR–ATLID synergy cloud product; and L2b ACM_CLP produces the CPR–ATLID–MSI synergy cloud product. The cloud microphysics scheme considers the maximum of two different size distributions at each JSG grid to treat and capture the coexistence of cloud and precipitation particles or particles with different cloud phases. For the EarthCARE mission, the outputs from the standard JAXA L2 cloud product feature a 3D global view of the dominant ice habit categories and microphysics and habit and size distribution transitions from cloud to precipitation. Demonstration of the JAXA L2 cloud particle category product using actual satellite data could show different preferences for the occurrence of different ice habit categories. Cloud particle formation and growth conditions can be examined further by incorporating EarthCARE radar Doppler velocity measurements.

The active-sensor-based JAXA L2 cloud products were assessed using simulated EarthCARE L1 orbit data created by the JAXA Joint Simulator, covering representative cloud and precipitation scenes across the globe. A comparison of retrieved and modeled microphysics obtained using the standard AC_CLP outputs as a reference showed that the retrieval reproduced the vertical profile of the modeled microphysics reasonably well, and the majority of the retrieved population of particle size and water content lay close to the 1 : 1 line, with the slopes of the regression lines around 0.8 for both the ice and liquid phases. Velocity-related products from the JAXA L2 research cloud product and further improvements in the microphysics retrieval from the CPR–ATLID–MSI synergy will be reported in a future study.

In addition to assessing the L2 cloud product using simulated EarthCARE L1 data, ongoing studies will characterize the product in the framework of JAXA EarthCARE calibration and validation activity. These studies include the use of ground-based radar and synergistic sensors at the NICT intensive observation site (Okamoto et al., 2024b), complementary data from other spaceborne sensors such as A-TRAIN (Sato and Okamoto, 2023), and a European Union–Japanese collaboration to evaluate CPR Doppler measurements and precipitation in CPR blind zones over Antarctica. As part of this joint activity, a validation methodology for spaceborne Doppler radar was developed to obtain an unattenuated 94 GHz Doppler spectrum and related information on particle shape, sedimentation velocity, and size distribution at high temporal resolution from a disdrometer and 24 GHz (K-band) Doppler radar synergy through frequency conversion and appropriate sampling strategies (Bracci et al., 2023). These validation datasets are highly valuable and will be used for further evaluation of the algorithms for EarthCARE, launched on 28 May 2024.

Data availability. The JAXA L2 Echo products, ATLID products, and MSI products were processed by the National Institute of Information and Communications Technology (PI: Hiroaki Horie), the National Institute for Environmental Studies (PI: Tomoaki Nishizawa), and Tokai University (PI: Takashi Nakajima), respectively. The standard products of the synthetic JAXA EarthCARE data are available from https://doi.org/10.5281/zenodo.7835229 (Roh et al., 2023b). The CALIPSO Level 1B profile data V4-10 and CloudSat 2B-GEOPROF P1_R05 data used in this study are provided from the Atmospheric Science Data Center at NASA's Langley Research Center (https://doi.org/10.5067/CALIOP/CALIPSO/LID_L1-STANDARD-V4-10; NASA/LARC/SD/ASDC, 2016) and the CloudSat Data Processing Center (https://www.cloudsat.cira.colostate.edu/data-products/2b-geoprof; Marchand and Mace, 2018), respectively. The KU CloudSat–CALIPSO merged dataset has been provided and updated to the latest version by the JAXA A-Train Product Monitor (https://www.eorc.jaxa.jp/EARTHCARE/A-train/A-train_monitor_e.html, JAXA/EORC, 2017).

Author contributions. KS conducted research and drafted the paper. KS and HO developed the L2 cloud algorithms. TN, YJ, RK, TYN, and MW processed the L1 data and produced the L2 products. MS and RW developed the synthetic EarthCARE data and provided the model outputs. HI provided scattering simulations. All authors provided useful discussions for the assessment of L2 cloud products.

Competing interests. The contact author has declared that none of the authors has any competing interests.

Disclaimer. Publisher's note: Copernicus Publications remains neutral with regard to jurisdictional claims made in the text, published maps, institutional affiliations, or any other geographical representation in this paper. While Copernicus Publications makes every effort to include appropriate place names, the final responsibility lies with the authors.

Special issue statement. This article is part of the special issue "EarthCARE Level 2 algorithms and data products". It is not associated with a conference.

Acknowledgements. The authors would like to thank the JAXA EarthCARE science team and the Remote Sensing Technology Center of Japan (RESTEC).

Financial support. This study was supported by the Japan Aerospace Exploration Agency (EORA3) for the EarthCARE mission (grant no. 24RT000193); JSPS KAKENHI (grant nos. JP22K03721 and JP24H00275); and the Research Institute for Applied Mechanics, Kyushu University (Fukuoka, Japan).

Review statement. This paper was edited by Robin Hogan and reviewed by two anonymous referees.

References

Baedi, R. J. P., De Wit, J. J. M., Russchenberg, H. W. J., Erkelens, J. S., and Poiares Baptista, J. P. V.: Estimating Effective Radius and Liquid Water Content from Radar and Lidar Based on the CLARE'98 Data-Set, Phys. Chem. Earth (B), 25, 1057–1062, https://doi.org/10.1016/S1464-1909(00)00152-0, 2000.

Borovoi, A., Konoshonkin, A., Kustova, N., and Okamoto, H.: Backscattering Mueller matrix for quasi-horizontally oriented ice plates of cirrus clouds: Application to CALIPSO signals, Opt. Express, 20, 28222–28233, https://doi.org/10.1364/oe.20.028222, 2012.

Bracci, A., Sato, K., Baldini, L., Porcù, F., and Okamoto, H.: Development of a methodology for evaluating spaceborne W-band Doppler radar by combined use of Micro Rain Radar and a disdrometer in Antarctica, Remote Sens. Environ., 294, 113630, https://doi.org/10.1016/j.rse.2023.113630, 2023.

Eisinger, M., Marnas, F., Wallace, K., Kubota, T., Tomiyama, N., Ohno, Y., Tanaka, T., Tomita, E., Wehr, T., and Bernaerts, D.: The EarthCARE mission: science data processing chain overview, Atmos. Meas. Tech., 17, 839–862, https://doi.org/10.5194/amt-17-839-2024, 2024.

Fox, N. I. and Illingworth, A. J.: The retrieval of stratocumulus cloud properties by ground-based cloud radar, J. Appl. Meteor., 36, 485–492, https://doi.org/10.1175/1520-0450(1997)036<0485:TROSCP>2.0.CO;2, 1997.

Fujiyoshi, Y.: Underlying Microphysical Processes in the Melting Layer during Moderate Precipitation: Evidence from Ground-Based Data, J. Atmos. Sci., 80, 1381–1400, https://doi.org/10.1175/JAS-D-22-0183.1, 2023.

Hagihara, Y., Okamoto, H., and Yoshida, R.: Development of a combined CloudSat-CALIPSO cloud mask to show global cloud distribution, J. Geophys. Res., 15, 1–17, https://doi.org/10.1029/2009JD012344, 2010.

Heymsfield, A. J., Bansemer, A., Wood, N. B., Liu, G., Tanelli, S., Sy, O. O., Poellot, M., and Liu, C.: Toward improving ice water content and snow-rate retrievals from radars. Part II: Results from three wavelength radar–collocated in situ measurements and CloudSat–GPM–TRMM radar data, J. Appl. Meteorol. Climatol., 57, 365–389, https://doi.org/10.1175/JAMC-D-17-0164.1, 2018.

Iguchi, T., Kozu, T., Meneghini, R., Awaka, J., and Okamoto, K.: Rain-Profiling Algorithm for the TRMM Precipitation Radar, J. Appl. Meteor., 39, 2038–2052, https://doi.org/10.1175/1520-0450(2001)040<2038:rpaftt>2.0.co;2, 2000.

Ishimoto, H.: Radar Backscattering Computations for Fractal-Shaped Snowflakes, J. Meteorol. Soc. Jpn., 86, 459–469, https://doi.org/10.2151/jmsj.86.459, 2008.

Ishimoto, H., Masuda, K., Mano, Y., Orikasa, N., and Uchiyama, A.: Irregularly shaped ice aggregates in optical modeling of convectively generated ice clouds, J. Quant. Spectrosc. Ra., 113, 632–643 https://doi.org/10.1016/j.jqsrt.2012.01.017, 2012.

JAXA (Japan Aerospace Exploration Agency)/EORC (Earth Observation Research Center): EarthCARE Research A-train Product Monitor, JAXA/EORC [data set], https://www.eorc.jaxa.jp/EARTHCARE/A-train/A-train_monitor_e.html, last access: 7 March 2025), 2017.

Jin, Y., Nishizawa, T., Sugimoto, N., Ishii, S., Aoki, M., Sato, K., and Okamoto, H.: Development of a 355-nm high-spectral-resolution lidar using a scanning Michelson interferometer for aerosol profile measurement, Opt. Express, 28, 23209–23222, https://doi.org/10.1364/oe.390987, 2020.

Jin, Y., Nishizawa, T., Sugimoto, N., Takakura, S., Aoki, M., Ishii, S., Yamazaki, A., Kudo, R., Yumimoto, K., Sato, K., and Okamoto, H.: Demonstration of aerosol profile measurement with a dual-wavelength high-spectral-resolution lidar using a scanning interferometer, Appl. Opt., 61, 3523–3532, 2022.

Khain, A., Pinsky, M., Magaritz, L., Krasnov, O., and Russchenberg, H.: Combined observational and model investigations of the Z-LWC relationship in stratocumulus clouds, J. Appl. Meteorol. Climatol., 47, 591–606, https://doi.org/10.1175/2007JAMC1701.1, 2008.

Kikuchi, M., Okamoto, H., Sato, K., Suzuki, K., Cesana, G., Hagihara, Y., Takahashi, N., Hayasaka, T., and Oki,

R.: Development of Algorithm for Discriminating Hydrometeor Particle Types With a Synergistic Use of CloudSat and CALIPSO, J. Geophys. Res.-Atmos., 122, 11022–11044, https://doi.org/10.1002/2017jd027113, 2017.

Krasnov, O. A. and Russchenberg, H. W. J.: The relation between the radar to lidar ratio and the effective radius of droplets in water clouds: An analysis of statistical models and observed drop size distributions, in: Proceedings of the 11th Conference in Cloud Physics, Ogden, Utah, United States of America, 2–7 June 2002, P2.18, https://ams.confex.com/ams/11AR11CP/techprogram/paper_42251.htm (last access: 6 March 2025), 2002.

Krasnov, O. A. and Russchenberg, H. W. J. R.: A synergetic radar-lidar technique for the LWC retrieval in water clouds: Description and application to the Cloudnet data, in: Proceedings of the 32nd Conference on Radar Meteorology, Albuquerque, New Mexico, United States of America, 24–29 October 2005, 11R.7, https://ams.confex.com/ams/32Rad11Meso/techprogram/paper_96496.htm (last access: 6 March 2025), 2005.

Kudo, R., Nishizawa, T., and Aoyagi, T.: Vertical profiles of aerosol optical properties and the solar heating rate estimated by combining sky radiometer and lidar measurements, Atmos. Meas. Tech., 9, 3223–3243, https://doi.org/10.5194/amt-9-3223-2016, 2016.

Kudo, R., Higurashi, A., Oikawa, E., Fujikawa, M., Ishimoto, H., and Nishizawa, T.: Global 3-D distribution of aerosol composition by synergistic use of CALIOP and MODIS observations, Atmos. Meas. Tech., 16, 3835–3863, https://doi.org/10.5194/amt-16-3835-2023, 2023.

Letu, H., Ishimoto, H., Riedi, J., Nakajima, T. Y., C.-Labonnote, L., Baran, A. J., Nagao, T. M., and Sekiguchi, M.: Investigation of ice particle habits to be used for ice cloud remote sensing for the GCOM-C satellite mission, Atmos. Chem. Phys., 16, 12287–12303, https://doi.org/10.5194/acp-16-12287-2016, 2016.

Li, M., Letu, H., Peng, Y., Ishimoto, H., Lin, Y., Nakajima, T. Y., Baran, A. J., Guo, Z., Lei, Y., and Shi, J.: Investigation of ice cloud modeling capabilities for the irregularly shaped Voronoi ice scattering models in climate simulations, Atmos. Chem. Phys., 22, 4809–4825, https://doi.org/10.5194/acp-22-4809-2022, 2022.

Marchand, R. and Mace, G.: Level 2 GEOPROF product process description and interface control document version P1_R05, CloudSat mission and the Data Processing Center (Cloud-Sat DPC) [data set], https://www.cloudsat.cira.colostate.edu/cloudsat-static/info/dl/2b-geoprof/2B-GEOPROF_PDICD.P1_R05.rev0__0.pdf (last access: 8 January 2024), 2018.

Marshall, J. S. and Palmer, W. McK.: The distribution of raindrops with size, J., Meteorol., 5, 165–166, 1948.

Masuda, K., Ishimoto, H., and Mano, Y.: Efficient method of computing a geometric optics integral for light scattering by nonspherical particles, Meteorol. Geophys., 63, 15–19, https://doi.org/10.2467/mripapers.63.15, 2012.

Nakajima, T. Y., Ishida, H., Nagao, T. M., Hori, M., Letu, H., Higuchi, R., Tamaru, N., Imoto, N., and Yamazaki, A.: Theoretical basis of the algorithms and early phase results of the GCOM-C (Shikisai) SGLI cloud products, Prog. Earth Planet Sci., 6, 52, https://doi.org/10.1186/s40645-019-0295-9, 2019.

NASA/LARC/SD/ASDC: CALIPSO Lidar Level 1B profile data, V4-10, NASA Langley Atmospheric Science Data Center DAAC [data set], https://doi.org/10.5067/CALIOP/CALIPSO/LID_L1-STANDARD-V4-10, 2016.

Nishizawa, T., Kudo, R., Oikawa, E., Higurashi, A., Jin, Y., Sugimoto, N., Sato, K., and Okamoto, H.: Algorithm to retrieve aerosol optical properties using lidar measurements on board the EarthCARE satellite, Atmos. Meas. Tech. Discuss. [preprint], https://doi.org/10.5194/amt-2024-100, in review, 2024.

Okamoto, H.: Information content of the 95-GHz cloud radar signals: Theoretical assessment of effects of nonsphericity and error evaluation of the discrete dipole approximation, J. Geophys. Res., 107, 4628, https://doi.org/10.1029/2001JD001386, 2002.

Okamoto, H., Sato, K., and Hagihara, Y.: Global analysis of ice microphysics from CloudSat and CALIPSO: incorporation of specular reflection in lidar signals, J. Geophys. Res., 115, D22209, https://doi.org/10.1029/2009JD013383, 2010.

Okamoto, H., Sato, K., Borovoi, A., Ishimoto, H., Masuda, K., Konoshonkin, A., and Kustova, N.: Interpretation of lidar ratio and depolarization ratio of ice clouds using spaceborne high-spectral-resolution polarization lidar, Opt. Express, 27, 36587–36600, https://doi.org/10.1364/oe.27.036587, 2019.

Okamoto, H., Sato, K., Borovoi, A., Ishimoto, H., Masuda, K., Konoshonkin, A., and Kustova, N.: Wavelength dependence of ice cloud backscatter properties for space-borne polarization lidar applications, Opt. Express, 28, 29178–29191, https://doi.org/10.1364/oe.400510, 2020.

Okamoto, H., Sato, K., Nishizawa, T., Jin, Y., Ogawa, S., Ishimoto, H., Hagihara, Y., Oikawa, E., Kikuchi, M., Satoh, M., and Roh, W.: Cloud masks and cloud type classification using EarthCARE CPR and ATLID, Atmos. Meas. Tech. Discuss. [preprint], https://doi.org/10.5194/amt-2024-103, in review, 2024a.

Okamoto, H., Sato, K., Nishizawa, T., Jin, Y., Nakajima, T., Wang, M., Satoh, M., Suzuki, K., Roh, W., Yamauchi, A., Horie, H., Ohno, Y., Hagihara, Y., Ishimoto, H., Kudo, R., Kubota, T., and Tanaka, T.: JAXA Level2 algorithms for EarthCARE mission from single to four sensors: new perspective of cloud, aerosol, radiation and dynamics, Atmos. Meas. Tech. Discuss. [preprint], https://doi.org/10.5194/amt-2024-101, in review, 2024b.

Roh, W., Satoh, M., Hashino, T., Matsugishi, S., Nasuno, T., and Kubota, T.: Introduction to EarthCARE synthetic data using a global storm-resolving simulation, Atmos. Meas. Tech., 16, 3331–3344, https://doi.org/10.5194/amt-16-3331-2023, 2023a.

Roh, W., Satoh, M., Hashino, T., Matsugishi, S., Nasuno, T., and Kubota, T.: The JAXA EarthCARE synthetic data using a global storm resolving simulation, Zenodo [data set], https://doi.org/10.5281/zenodo.7835229, 2023b.

Sato, K. and Okamoto, H.: Refinement of global ice microphysics using spaceborne active sensors, J. Geophys. Res., 116, D20202, https://doi.org/10.1029/2011JD015885, 2011.

Sato, K. and Okamoto, H.: Application of single and multiple-scattering theories to analysis of space-borne cloud radar and lidar data, Springer Nature, Springer Series in Light Scattering, in: Springer series in light scattering, edited by: Kokhanovsky, A., Springer, Cham, 1–37, https://doi.org/10.1007/978-3-030-38696-2_1, 2020.

Sato, K. and Okamoto, H.: Global Analysis of Height-Resolved Ice Particle Categories From Spaceborne Lidar, Geophys. Res. Lett.,

50, e2023GL105522, https://doi.org/10.1029/2023gl105522, 2023.

Sato, K., Okamoto, H., Yamamoto, M. K., Fukao, S., Kumagai, H., Ohno, Y., Horie, H., and Abo, M.: 95-GHz Doppler radar and lidar synergy for simultaneous ice microphysics and in-cloud vertical air motion retrieval, J. Geophys. Res., 114, D03203, https://doi.org/10.1029/2008JD010222, 2009.

Sato, K., Okamoto, H., Takemura, T., Kumagai, H., and Sugimoto N.: Characterization of ice cloud properties obtained by ship-borne radar/lidar over the tropical western Pacific Ocean for evaluation of an atmospheric general circulation model, J. Geophys. Res., 115, D15203, https://doi.org/doi:10.1029/2009JD012944, 2010

Sato, K., Okamoto, H., Ishimoto, H.: Physical model for multiple scattered space-borne lidar returns from clouds, Opt. Express, 26, A301–A319, https://doi.org/10.1364/OE.26.00A301, 2018.

Sato, K., Okamoto, H., and Ishimoto, H.: Modeling the depolarization of space-borne lidar signals, Opt. Express, 27, A117–A132, https://doi.org/10.1364/OE.27.00A117, 2019.

Satoh, M., Tomita, H., Yashiro, H., Miura, H., Kodama, C., Seiki, T., Noda, A. T., Yamada, Y., Goto, D., Sawada, M., Miyoshi, T., Niwa, Y., Hara, M., Ohno, T., Iga, S., Arakawa, T., Inoue, T., and Kubokawa, H.: The Non-hydrostatic Icosahedral Atmospheric Model: description and development, Prog. Earth Planet. Sci., 1, 18, https://doi.org/10.1186/s40645-014-0018-1, 2014.

Sullivan, S., Lee, D., Oreopoulos, L., and Nenes, A.: Role of updraft velocity in temporal variability of global cloud hydrometeor number, P. Natl. Acad. Sci. USA, 113, 5791–5796, https://doi.org/10.1073/pnas.1514039113, 2016.

Van Diedenhoven, B.: Remote sensing of crystal shapes in ice clouds, in: Springer series in light scattering, Springer series in light scattering, edited by: Kokhanovsky, A., Springer, Cham, 197–250, https://doi.org/10.1007/978-3-319-70808-9_5, 2018.

Wang, M., Nakajima, T. Y., Roh, W., Satoh, M., Suzuki, K., Kubota, T., and Yoshida, M.: Evaluation of the spectral misalignment on the Earth Clouds, Aerosols and Radiation Explorer/multi-spectral imager cloud product, Atmos. Meas. Tech., 16, 603–623, https://doi.org/10.5194/amt-16-603-2023, 2023.

Yamauchi, A., Suzuki, K., Oikawa, E., Sekiguchi, M., Nagao, T. M., and Ishida, H.: Description and validation of the Japanese algorithm for radiative flux and heating rate products with all four EarthCARE instruments: pre-launch test with A-Train, Atmos. Meas. Tech., 17, 6751–6767, https://doi.org/10.5194/amt-17-6751-2024, 2024.

Yoshida, R., Okamoto, H., Hagihara, Y., and Ishimoto, H.: Global analysis of cloud phase and ice crystal orientation from Cloud-Aerosol Lidar and Infrared Pathfinder Satellite Observation (CALIPSO) data using attenuated backscattering and depolarization ratio, J. Geophys. Res., 115, D00H32, https://doi.org/10.1029/2009jd012334, 2010.